Structural, Elastic and Electronic Properties of γ″ Phase Precipitate in Mg-Gd-Zn Alloy

[1]Mengmeng Wu, [2]Rongkai Pan, [1]Jilei Liang*, [1]Guohai Zhou, [3]Li Ma and [1]Chunyu Zhang
[1]College of Pharmacy and Chemistry &Chemical Engineering, Jiangsu Key Laboratory of Chiral Pharmaceuticals Biosynthesis, Taizhou University, Taizhou 225300, P. R. China.
[2]Department of Materials, Yantai Nanshan University, Yantai 265713, P. R. China.
[3]Key Laboratory of New Electric Functional Materials of Guangxi Colleges and Universities, Guangxi Teachers Education University, Nanning 530023, P. R. China.
liangjilei_httplan@126.com*

(Received on 28th February 2018, accepted in revised form 20th December 2018)

Summary: The γ″ phase (Mg_4GdZn) precipitate in Mg-Gd-Zn alloy was calculated via first-principle density functional theory within the generalized gradient approximation. Through structure optimization of full relaxation, the lattice parameters were theoretically obtained, and the calculated Mg_4GdZn is the most energetically stable in view of the formation energy. Independent elastic constants were also calculated, illustrating the calculated Mg_4GdZn is mechanically stable. The shear modulus, polycrystalline bulk modulus, Poisson ratio, and Young's modulus of Mg_4GdZn were calculated via the Voigt-Reuss-Hill approximation. Elastic anisotropy and ductility were analyzed in details. Seen from their charge density distribution and electronic density of states, both metallic bond and covalent bond were found in Mg_4GdZn.

Keywords: First-principles calculations; Elastic properties; Elastic anisotropy; Electronic structure; γ" phase; Mg_4GdZn.

Introduction

Various rare-earth-containing magnesium alloys, for example, Mg-Y-Nd, Mg-Gd-Y, and Mg-Gd-Nd, have been receiving more and more attention in recent years due to their better creep resistance and higher strength [1-9]. For the Mg-Gd-based systems, β' and β_1 are the key strengthening precipitate phases, and the precipitation sequence and structure, morphology of these phases in the mentioned systems have been relatively established. For binary Mg-Gd alloy with content of Gd<1.4 at.%, it shows little age hardening response. The phenomenon is resulted from the lack of obvious volume fraction of precipitates and even the rare distribution of coarse precipitates. Fortunately, the addition of slight amount of Zn (0.5-0.7 at.%) could produce an intensive precipitation hardening response and sharply increase the alloy creep resistance [10]. Moreover, the hardness of the alloy is also greatly enhanced (~17 VHN), even when quenching. The improvement of the alloy is remarkable when the content of Zn is 0.4 at.%. A recent study has demonstrated that the enhancement of age hardening response results from a denser distribution of γ″ phase precipitate that is not found in binary Mg-Gd alloy.

Through the 3-dimensional atom probe and selected area electron diffraction analysis, Nie has proposed Mg_4GdZn as the chemical composition of γ″ phase precipitate, and constructed a hexagonal unit cell as the concrete structure model [11]. Based on the crystal structure in α-Mg, Nie has deduced an ordered hexagonal structure (space group P62m, a = 5.60 Å, c = 4.44 Å) of the γ″ phase. However, the result has not been confirmed, no matter theoretically or experimentally. Besides, as a key strengthening phase in the Mg-based alloy, the γ″ precipitate has great significance in optimizing the micro-structure and enhancing their mechanical properties. Unfortunately, the investigation about the γ″ precipitate is relatively rare. Therefore, further theoretical and experimental studies are imperative.

In this paper, theoretical calculations based on first-principle within the generalized gradient approximation (GGA) were performed to study the elastic property and electronic structure of the γ″ phase (Mg_4GdZn) in Mg-Gd-Zn system. The results were analyzed and compared to the experimental data reported in literatures, which can provide references for the rational design and optimization of Mo-based alloys.

Experimental

Calculations were completed through the Vienna Ab Simulation Package [12]. The Perdew-Wang (PW91) version of the GGA [13] and the projector augmented wave method [14] were adopted. The cutoff

*To whom all correspondence should be addressed.

energy for the plane wave basis set was 360 eV and Gamma centered Monkhors-Pack grids with 12×12×15 for the BZ integration were adopted [15].

Elastic constants were obtained through the calculation of the total energy as a function of proper lattice deformation, and internal energy E (V, ε) for the slightly deformed crystal is calculated by Equation (1) [16].

$$E(V,[\varepsilon_{mn}]) = E(V_0,0) + \frac{V_0}{2}\sum_{i,j=1}^{6} c_{ij}\varepsilon_i\varepsilon_j \qquad (1)$$

where $E(V_0, 0)$ is the total energy in equilibrium, and ε_i and ε_j are strains with Voigt's notation.

The five independence elastic constants were calculated through fitting the energy-strain profiles with quadratic polynomial which can be found in details in Ref. [17-19].

Results and Discussion

Crystal structure and stability

Mg_4GdZn shows a hexagonal structure with a $P62m$ space group. Based on the structure model proposed by Nie [11], we performed the structure optimization through the relaxation of internal atom positions and unit cell shape. The equilibrium lattice parameters of Mg_4GdZn are a=b=5.646 Å, c=4.783 Å. In comparison with the experimental value (a=b=5.60 Å, c=4.44 Å, see Ref. [11]), the present theoretical lattice parameters a and b are in accordance with the expected value from the structure model, while c is larger evidently. The reason lies in the different atom radii of Mg (1.60 Å) and Gd (1.88 Å). Hence, the lattice parameters of the alloys will change due to the addition of Gd. The obtained results here will shed a light on the further theoretical and experimental investigation of the alloy. In addition, a series of total energies per unit cell were also obtained and fitted by the Birch-Murnaghan equation of state (EOS) [19]. The volume V_0 and bulk modulus B_0 are 138.6 Å^3 and 42.54 GPa, respectively.

The formation energy was further calculated by Equation (2) in order to investigate the structure stability of the Mg_4GdZn. The obtained formation energy for Mg_4GdZn is -0.084 eV/atom, and the negative formation energy proves the formation stability of Mg_4GdZn.

$$\Delta H = \frac{E_{tot} - N_A E_{solid}^A - N_B E_{solid}^B - N_C E_{solid}^C}{N_A + N_B + N_C} \qquad (2)$$

Elastic properties

Table-1 showed the calculated elastic constants which can provide useful information of bonds in the material and are closely related to the mechanical properties. In Mg_4GdZn, the elastic constant C_{11} is less than C_{33}. On one hand, it illustrates the weaker bond strength along directions [1010] and [0110] than that along [0001]. On the other hand, C_{11}+C_{12}>C_{33} implies the higher elastic modulus in (0001) plane than along c-axis [20]. Besides, C_{44} is higher than C_{66}, indicating that the easier shear of [1010] (0110) than that of [1010] (0001). The mechanical stability criteria of hexagonal lattice are C_{11}, C_{11}-C_{12}, C_{44} and (C_{11}+C_{12})C_{33}-2C_{13}^2 must be positive [21]. The calculated elastic constants of Mg_4GdZn obeyed are in line with the criteria, illustrating the mechanical stability of Mg_4GdZn.

The polycrystalline elastic modulus was also determined [22]. For the hexagonal cell, the Voigt limits of G (G_V) and B (B_V) are shown in Equations (3-4).

$$G_V = \frac{1}{30}\left(7C_{11} - 5C_{12} + 12C_{44} + 2C_{33} - 4C_{13}\right) \qquad (3)$$

$$B_V = \frac{2}{9}\left(C_{11} + C_{12} + C_{33}/2 + 2C_{13}\right) \qquad (4)$$

And the Reuss bounds (G_R and B_R) are shown in Equations (5-6).

$$G_R = \frac{5}{2}\left\{\frac{[(C_{11}+C_{12})C_{33} - 2C_{13}^2]C_{44}C_{66}}{3B_V C_{44}C_{66} + [(C_{11}+C_{12})C_{33} - 2C_{13}^2](C_{44}+C_{66})}\right\} \qquad (5)$$

$$B_R = \frac{(C_{11}+C_{12})C_{33} - 2C_{13}^2}{C_{11} + C_{12} + 2C_{33} - 4C_{13}} \qquad (6)$$

Table-1: Single crystal elastic constants c_{ij} (in GPa), elastic modulus (in GPa) and Poisson's ratio v of Mg_4GdZn.

C_{11}	C_{12}	C_{33}	C_{13}	C_{44}	C_{66}	C_{11}-C_{12}	B	G	Y	v
68.86	**31.77**	**86.28**	**29.93**	**34.06**	**18.55**	**37.09**	**45.07**	**25.22**	**63.76**	**0.26**

Ultimately, the mean values of VRH are calculated by Equations (7-8).

$$B = \frac{1}{2}(B_V + B_R) \quad (7)$$

$$G = \frac{1}{2}(G_V + G_R) \quad (8)$$

where the subscripts *V* and *R* are the Voigt and Reuss bounds, respectively. Furthermore, the Young's modulus *Y* and Poisson's ratio υ are calculated according to Equations (9-10).

$$Y = \frac{9BG}{3B+G} \quad (9)$$

$$\nu = \frac{3B-2G}{2(3B+G)} \quad (10)$$

The calculated results were also shown in Table-1. It is noted that the obtained bulk modulus of Mg_4GdZn is in accordance with that obtained by fitting to the Birch-Murnaghan EOS. Elastic moduli can determine the hardness of material. Elastic moduli include bulk modulus, shear modulus and Young's modulus [23, 24]. Fig. 1 showed the obtained shear modulus, bulk modulus and Young's modulus comparing with the corresponding experimental values in single-crystal Mg [25]. The obtained bulk modulus of Mg_4GdZn is higher obviously than the experimental value of Mg, and the enhancement implies higher hardness of the material, which is in line with the reported experiment values [11]. Besides, the evident enhancements of Young's modulus and shear modulus of Mg_4GdZn were also found, indicating the better mechanical property in Mg_4GdZn.

Pugh proposed a general *B/G* criterion to predict the ductility or brittleness of material [26]. A higher *B/G* value is related to ductility, and the criterion distinguishing ductility and brittleness is 1.75. Actually, the obtained value of *B/G* for Mg_4GdZn is 1.79, slightly higher than the criterion, indicating that Mg_4GdZn is ductile. Meanwhile, C_{11}-C_{12} is also a very significant indicator of the mechanical property [27]. The smaller of C_{11}-C_{12}, the better of the plasticity. As shown in Table-1, the C_{11}-C_{12} of Mg_4GdZn is lower than that of Mg, implying a good plasticity. Finally, the smaller Poisson's ratio in Table-1 also demonstrated the stability of Mg_4GdZn.

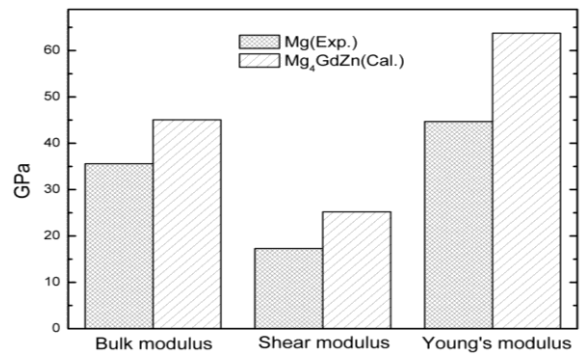

Fig. 1: The elastic modulus of Mg (the experimental data from Ref. [25]) and Mg_4GdZn (the calculated values in the present work).

Elastic anisotropy

The elastic anisotropy of materials is related to the occurrence of micro-cracks [28]. Actually elastic anisotropic behavior is found in all of the known crystals. Hence, it is necessary to quantify the elastic anisotropy of Mg_4GdZn. Here, the anisotropy of Mg_4GdZn was discussed based on several criteria.

For hcp system, the linear bulk moduli B_a and B_c along *a*- and *c*-axe, respectively, are defined as Equations (11-14) [29], and the value of 1 demonstrates elastic isotropy of the material. The calculated B_a and B_c in Table-2 showed that the bulk moduli of Mg_4GdZn deviate from isotropy in these two directions.

$$B_a = a\frac{dp}{da} = \frac{\Lambda}{2+\beta} \quad (11)$$

$$B_c = c\frac{dp}{dc} = \frac{B_a}{\beta} \quad (12)$$

where

$$\Lambda = 2(C_{11} + C_{12}) + 4C_{13}\beta + C_{33}\beta^2 \quad (13)$$

$$\beta = \frac{C_{11} + C_{12} - 2C_{13}}{C_{33} - C_{13}} \quad (14)$$

Table-2: Shear anisotropic factors, linear bulk modulus Ba (in GPa) and Bc (in GPa), and the percent of anisotropy in the compression AB and shear AG (in %).

Material	$A_{\{10\bar{1}0\}}$	$A_{\{01\bar{1}0\}}$	$A_{\{0001\}}$	$A_G(\%)$	$A_B(\%)$	B_a	B_c	$1/\beta$
Mg_4GdZn	**1.429**	**1.429**	**1.0**	**3.731**	**0.390**	**122.275**	**169.022**	**1.382**

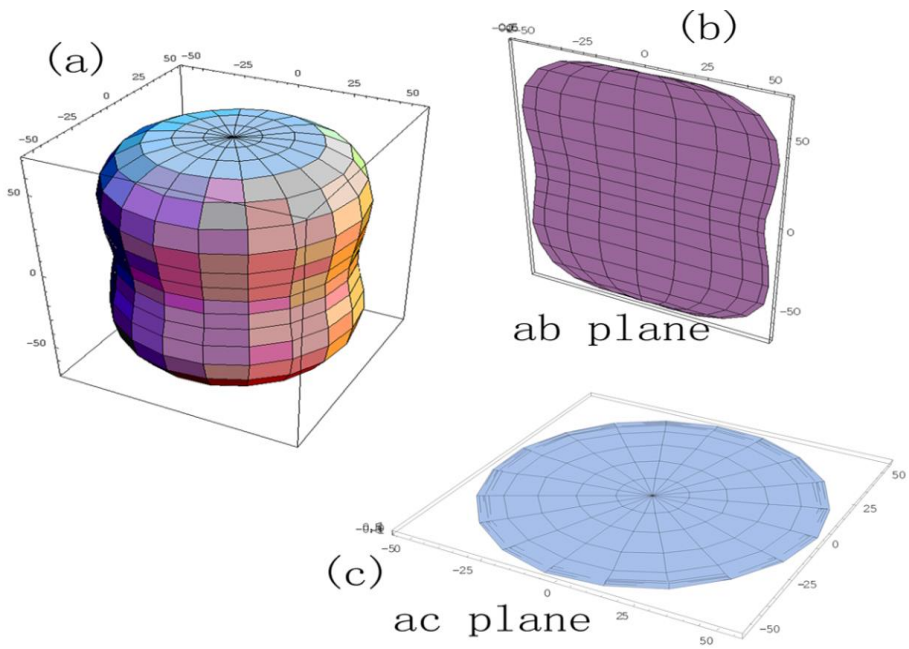

Fig. 2: (a) Directional dependence of Young's modulus, (b) and (c) plane projections of the directional dependence of Young's modulus in Mg_4GdZn (in GPa).

The elastic anisotropy in compressibility and shear could be also qualified by two dimensionless quantities $A_B = (B_V - B_R)/(B_V + B_R)$ and $A_G = (G_V - G_R)/(G_V + G_R)$, respectively [30-31]. The value of 0 means elastic isotropy while 1 shows the largest possible anisotropy. The calculated A_B and A_G are 0.39% and 3.73%, respectively, indicating a small anisotropy in Mg_4GdZn.

To further describe the elastic anisotropy of Mg_4GdZn, it is necessary to study the in-plane anisotropy. For hexagonal symmetry cell, the in-plane anisotropy of *a-b* doesn't exist while that of *a-c* exists [32]. Besides, the directional dependence of Young's modulus 1/Y, which is defined as Equation (15) [21], can also describe the in-plane elastic anisotropy.

$$\frac{1}{Y} = (1-l_3^2)^2 s_{11} + l_3^4 s_{33} + l_3^2(1-l_3^2)(2s_{13} + s_{44}) \qquad (15)$$

The 1/Y was calculated and shown in Fig. 2. For an isotropic system, 1/Y is spherical shape. However, the nonspherical nature of 1/Y of Mg_4GdZn in Fig. 2 clearly showed the anisotropy in the *ac* plane.

Electronic structures

In this paper, the electronic structure was also obtained to provide a better understanding of the bonding characteristic of Mg_4GdZn, and to further interpret the mechanism of elastic property and structure stability of the Mg_4GdZn. The DOS of Mg_4GdZn was presented in Fig. 3, consisting of the DOS of Mg, Gd and Zn. Seen from the partial and total DOS shown in Fig. 3, Mg_4GdZn exhibits metallic behavior. The total DOS near the Fermi level is mainly the Mg-p, Gd-d and Zn-p states, while the Gd-p and Gd-s states are weak. Near the Fermi level, a strong hybridization of Mg-p states with Zn-p, Gd-d states is found. In addition, a quasigap near the Fermi level is also found, indicating the formation of the directional covalent bond [33]. The covalent bond can raise the material strength compared to the metallic bond. Hence, the quasigap near the Fermi level indicates a pronounced stability in the alloy.

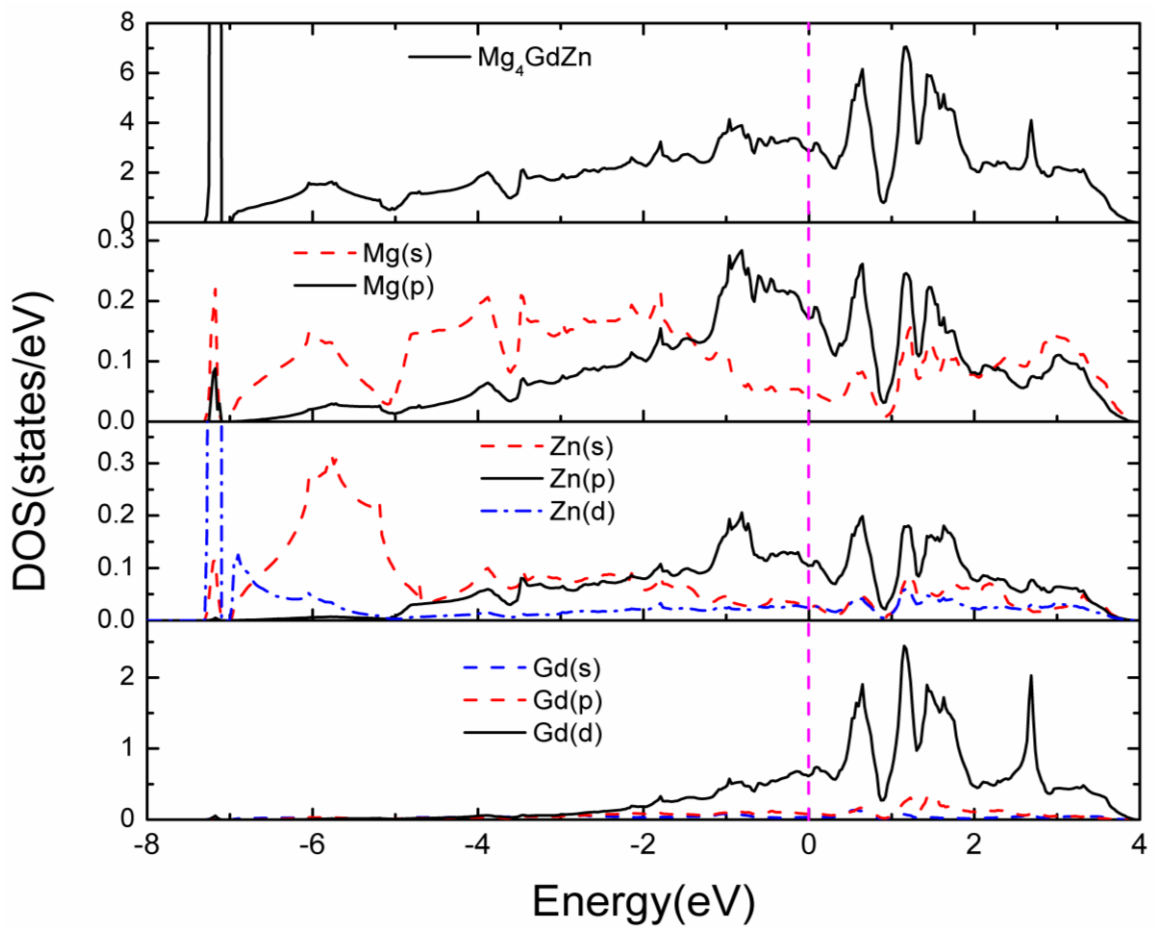

Fig. 3: The total and partial density of states of Mg_4GdZn in which the Fermi level is set at zero energy and marked by the vertical dot line.

The charge density distribution of Mg_4GdZn in the plane (1121) was presented in Fig. 4. The contour lines were plotted from 0.02 to 0.22 eV/Å^3. The high charge accumulation between Zn and Gd atoms, together with the aspherical shape indicated directional covalent bond between the atoms. Different from the Zn-Gd bond, no overlaps of electron distribution around Mg atoms are found. Hence, the electron distribution near Mg atoms is almost metal-like bond, which is in line with the DOS analysis.

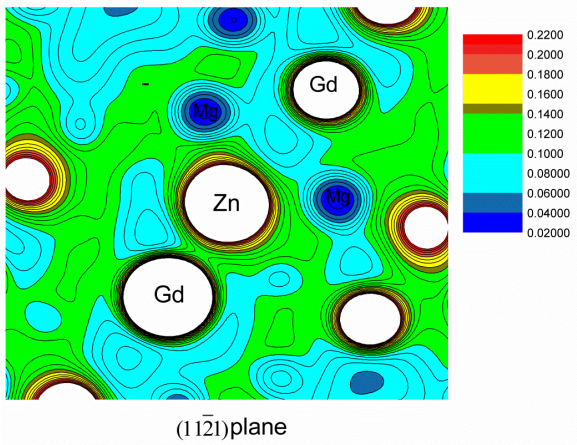

Fig. 4: The charge density distribution map on (1121) plane for Mg_4GdZn in which the contour lines are plotted from 0.02 to 0.22 e/Å^3 with 0.01 e/Å^3 intervals.

Conclusion

In this paper, the structural, mechanical and electronic properties of Mg_4GdZn in Mg-Gd-Zn alloy were studied through DFT within the GGA. The lattice parameters of Mg_4GdZn were calculated theoretically, and the formation enthalpy indicates that Mg_4GdZn is energetically stable. The calculated five independent elastic constants proved that Mg_4GdZn is mechanically stable. The elastic anisotropy and the electronic properties were discussed in details. These results can provide references for the rational design and optimization of Mo-based alloys.

Acknowledgements

Financial support from State Key Laboratory of Heavy Oil Processing (SKLOP201902005), Natural Science Foundation of Jiangsu Higher Education Institutions of China (18KJB580016, 17KJB530009), and Taizhou City Science and Technology Supporting Program (TS201627) are gratefully acknowledged.

References

1. K. Hagihara, T. Okamoto, and M. Yamasaki, Electron backscatter diffraction pattern analysis of the deformation band formed in the Mg-based long-period stacking ordered phase, *Scripta. Mater.*, **117**, 32(2016).
2. X. D. Li, H. T. Ma, Z. H. Dai, Y. C. Qian, L. J. Hu, and Y. P. Xie, First-principles study of coherent interfaces of Laves-phase $MgZn_2$ and stability of thin $MgZn_2$ layers in Mg-Zn alloys, *J. Alloy. Compd.*, **696**, 109(2017).
3. M. M. Wu, B. Y. Tang, L. M. Peng, and W. J. Ding. Elastic and electronic properties of $ScMn_2$ from first-principles calculations, *Physica B*, **405**, 4812(2010).
4. H. S. Jang, K. M. Kim, and B. J. Lee, Modified embedded-atom method interatomic potentials for pure Zn and Mg-Zn binary system, *Calphad*, **60,** 200(2018).
5. Z. Li, Z. Zhao, Z. Zhou, H. Wang, and S. Li, First-principles calculations on small Mg_nZn and $Mg_{n-1}Zn_2$ clusters: Structures, stability, electronic properties, *Mater. Chem. Phys.*, **199**, 585(2017).
6. Y. Huang, X. F. Guo, Y L. Ma, H B. Shao, and Z B. Xiao, Stabilities, electronic and elastic properties of L_{12}-$Al_3(Sc_{1-x},Zr_x)$ with different Zr content: A first-principles study, *Physica B*, **548**, 27(2018).
7. Q. Yu, J. Wang, and Y. Jiang, Twin-twin interactions in magnesium, *Acta Mater.*, **77**, 28(2014).
8. M. M. Wu, Y. Jiang, J. W. Wang, J. Wu, B. Y. Tang, L. M. Peng, and W. J. Ding, Structural, elastic and electronic properties of $Mg(Cu_{1-x}Zn_x)_2$ alloys calculated by first-principles, *J. Alloy. Compd.*, **509**, 2885(2011).
9. J. F. Nie, Y. M. Zhu, and A. J. Morton, On the structure, transformation and deformation of long-period stacking ordered phases in Mg-Y-Zn alloys, *Metall. Mater. Transa.*, **45**,3338(2014).
10. J. F. Nie, X. Gao, and S. M. Zhu, Enhanced age hardening response and creep resistance of Mg-Gd alloys containing Zn, *Scripta. Mater.*, **53**, 1049(2005).
11. J. F. Nie, K. Ohishi, X. Gao, and K. Hono, Solute segregation and precipitation in a creep-resistant Mg-Gd-Zn alloy, *Acta Mater.*, **56**, 6061(2008).
12. G. Kresse, and J. Furthmüller, Efficient iterative schemes for ab initio total energy calculations using a plane-wave basis set, *Phys. Rev. B*, **54**, 11169(1996).
13. J. P. Perdew, J. A. Chevary, S. H. Vosko, K. A. Jackson, M. R. Pederson, D. J. Singh, and C. Fiolhais, Atoms, molecules, solids, and surfaces: applications of the generalized gradient approximation for exchange and correlation, *Phys. Rev. B*, **46**, 6671(1992).
14. P. E. Blöchl, Projector augmented-wave method, *Phys. Rev. B*, **50**, 17953(1994).
15. H. J. Monkhorst, and J. D. Pack. Special points for Brillouin-zone integrations, *Phys. Rev. B*, **13**, 5188(1976).
16. D. C. Wallace. *Thermodynamics of Crystals*, Wiley, New York, p. 222(1972).
17. X. H. Deng, B. B. Fan, and W. Lu, First-principles investigations on elastic properties of α- and β-Ta_4AlC_3, *Solid State Commun.*, **149**, 441(2009).
18. R. Ueji, N. Tsuchida, D. Terada, N. Tsujic, Y. Tanaka, A. Takemura, and K. Kunishige, Tensile properties and twinning behavior of high manganese austenitic steel with fine-grained structure, *Scripta. Mater.*, **59**, 963(2008).
19. M. M. Wu, L. Wen, B. Y. Tang, L. M. Peng, and W. J. Ding, First-principles study of elastic and electronic properties of $MgZn_2$ and $ScZn_2$ phases in Mg-Sc-Zn alloy, *J. Alloy. Compd.*, **506**, 412(2010).
20. X. Tao, P. Jund, C. Colinet, and J. Tédenac, First-principles study of the structural, electronic and elastic properties of W_5Si_3, *Intermetallics*, **18**,

688(2009).

21. L. Wang, P. Eisenlohr, and Y. Yang, Nucleation of paired twins at grain boundaries in titanium, *Scripta. Mater*., **63**, 827(2010).
22. J. Kacher, and A. M. Minor, Twin boundary interactions with grain boundaries investigated in pure rhenium, *Acta Mater.*, **81**, 1(2014).
23. A. F. Young, C. Sanloup, E. Gregoryanz, S. Scandolo, R.J .Hemley, and H. K. Mao, Synthesis of novel transition metal nitrides IrN_2 and OsN_2, *Phys. Rev. Lett.*, **96**, 155501(2006).
24. B. Yin, Z. Wu, and W. A. Curtin, First-principles calculations of stacking fault energies in Mg-Y, Mg-Al and Mg-Zn alloys and implications for <c+a> activity, *Acta Mater.*, **136,** 249(2017).
25. F. Cardarelli, *Materials Handbook*, Springer, London, p 125(2000).
26. A. Sumer, and J. F. Smith, Elastic constants of single-crystal $CaMg_2$, *J. Appl. Phys.*, **33**, 2283(1962).
27. C. Lou, X. Zhang, and Y. Ren, Non-schmid-based {10-12} twinning behavior in polycrystalline magnesium alloy, *Mater. Charact.*, **107**, 249(2015).
28. F. Wang, S. J. Sun, B. Yu, F. Zhang, P. L. Mao, and Z. Liu, First principles investigation of binary intermetallics in Mg-Al-Ca-Sn alloy: Stability, electronic structures, elastic properties and thermodynamic properties, T. Nonferr. Metal Soc., **26,** 203(2016).
29. S. Qun, X. Y. Zhang, and Y. Ren, Observations on the intersection between twin variants sharing the same zone axis in deformed magnesium alloy, *Mater. Charact.*, **109**, 160(2015).
30. D. H. Chung, and W. R. Buessem, *Anisotropy in Single Crystal Refractory Compound*, Plenum, New York, p 217(1968).
31. K. B. Panda, and K. SR Chandran, Determination of elastic constants of titanium diboride (TiB_2) from first principles using FLAPW implementation of the density functional theory, *Comput. Mater. Sci.*, **35**, 134(2006).
32. R. Matsumoto, and M. Uranagase, Deformation analysis of the long-period stacking-ordered phase by using molecular dynamics simulations: kink deformation under compression and kink boundary migration under tensile strain, *Mater. Transact.*, **56**, 957(2015).
33. A. Issa, J. E. Saal, and C. Wolverton, Formation of high-strength β′ precipitates in Mg-RE alloys: The role of the Mg/β″ interfacial instability, *Acta Mater.*, **83,** 75(2015).